Available online at www.sciencedirect.com
ScienceDirect
Journal of Magnetic Resonance 187 (2007) 184–192
JMR Journal of Magnetic Resonance
www.elsevier.com/locate/jmr

Real-time imaging of the spatial distribution of rf-heating in NMR samples during broadband decoupling

Reinhard Wimmer [a], Gerhard Wider [b,*]

[a] Department of Biotechnology, Chemistry and Environmental Engineering, Aalborg University, Sohngaardsholmsvej 49, DK-9000 Aalborg, Denmark
[b] Institute of Molecular Biology and Biophysics, ETH Zurich, CH-8093 Zurich, Switzerland

Received 22 January 2007; revised 16 April 2007
Available online 3 May 2007

Abstract

Continuous radio-frequency (rf) irradiation during decoupling and spin-lock periods in NMR pulse sequences may lead to undesired sample heating. Heat-sensitive samples can suffer damage from the sudden temperature rise which cannot be adequately compensated by the temperature control system. Moreover, as the heating is spatially inhomogeneous, higher temperature increases can arise locally than are indicated by the average increase detected by the temperature controller. In this work we present a technique that allows measurement of a real-time 2D-image of the temperature distribution inside an NMR sample during an experiment involving rf-heating. NMR imaging methods have previously been used to project the temperature distribution inside an NMR sample onto a single spatial axis or to acquire steady-state 2D- temperature distributions. The real-time 2D-temperature profiles obtained with our procedure provide much more detailed data. Our results show, that not only inhomogeneous heating but also inhomogeneous sample cooling contribute to the build-up of temperature gradients across the sample. The technique can be used to visualize rf-heating in order to protect sensitive samples and to experimentally test new coil geometries or to guide probehead design.

Keywords: Solution NMR; rf-Heating; Temperature imaging; Spatially resolved temperature measurement; NMR thermometer

1. Introduction

Sample heating by radio-frequency (rf) irradiation is a well-known phenomenon in NMR spectroscopy. rf-heating is caused by the interaction of the dipoles and ions in the sample with the electric field component of the electromagnetic rf-field used to excite the spins. The dielectric loss in the sample leads to longer rf pulses and rf-heating. These effects are highly undesirable, e.g. minimal heating of the living ''samples'' has to be ensured. in medical imaging and *in vivo* NMR; and in high-resolution NMR temperature gradients across the sample lead to convective flows which may cause the NMR-signal to deteriorate [1–5]. Furthermore, temperature gradients in a sample can lead to reduced accuracy in the physical parameters determined by NMR [2]. When temperature-dependent chemical shifts are observed, an inhomogeneous temperature distribution can have a similar effect as an inhomogeneous magnetic field. Receiver and transmitter coils in NMR probes are therefore designed to minimize the occurrence of electrical fields within the sample volume and thereby to minimize dielectric losses. This minimization is currently obtained with numerical simulations; experimental verification of the results has been difficult. Therefore it was desirable to develop a method for spatial mapping of electric field (E-field) components in a sample that would allow an efficient testing of new coil geometries and an experimental verification of the numerical simulations.

Since electric fields manifest themselves by rf-heating, the E-field distribution in the sample can be determined by imaging the temperature distribution in real-time during an experiment involving strong rf-heating. Loening

* Corresponding author. Fax: +41 1 633 1073.
E-mail address: gsw@mol.biol.ethz.ch (G. Wider).

1090-7807/$ - see front matter © 2007 Elsevier Inc. All rights reserved.
doi:10.1016/j.jmr.2007.04.014

and Keeler [2] have published a method to measure the temperature distribution along the z-axis of an NMR sample after reaching the steady-state in a broadband decoupling sequence and to image the resulting convective flow. In a later publication the same authors measured the transverse temperature profile across an NMR sample tube after rf-heating [6]. The steady-state temperature distribution they obtained may result from two processes: inhomogeneous heating and inhomogeneous cooling, but the two contributions cannot be separated. The target of the present paper is to separate these two contributions and to assess the inhomogeneity both of rf-heating and of sample cooling. Therefore a method is needed that can map the temperature changes during an NMR experiment spatially resolved and in real-time.

Several compounds with temperature-dependent chemical shifts have been reported as NMR-thermometers, involving ^{1}H, ^{2}H, ^{19}F, ^{13}C, ^{31}P [7] and ^{129}Xe [8]. One of the most temperature-sensitive NMR resonances is observed for ^{59}Co [9], which can easily be measured in highly symmetric complexes like hexacyanocobaltate(III), $Co(CN)_6^{3-}$. For our purpose, a spectrum with only one signal is desirable, thus we chose ^{59}Co as an NMR thermometer. The gyromagnetic ratio of ^{59}Co is close to that of ^{13}C and its natural abundance is 100%. Thus, the sensitivity of ^{59}Co is reasonably good, so that spatially resolved chemical shift (and thereby temperature) measurements on ^{59}Co are feasible.

2. rf-Heating

The oscillating magnetic and electric field components of rf radiation interact with the magnetic and electric dipoles of the sample molecules, respectively. In standard NMR samples, i.e. aqueous or organic solutions, the interaction between magnetic dipoles and oscillating magnetic fields are very weak and can be neglected [10]. In contrary, the interactions between the electric field components and the electric dipoles or ions in a solution are strong and can lead to serious dielectric losses which manifest themselves as sample heating. Two different kinds of interaction partners have to be considered: permanent dipoles and ions. Permanent dipoles will reorient according to the oscillating electric field as long as its frequency is small enough. At increasing frequency the dipoles will lag behind the oscillations of the electric field and their orientation will stay behind the orientation of the electric field. This phase lag leads to a conversion of electric field energy into heat and to decreasing orientation polarization which causes a decreasing dielectric constant of the sample. The energy absorbed by the dipoles per unit volume and per time becomes [10]

$$W = \tfrac{1}{2}\varepsilon''\omega E_0^2 \tag{1}$$

where E_0 is the strength and ω the frequency of the oscillating electric field, ε'' is the dielectric loss given by

$$\varepsilon'' = \frac{(\varepsilon_0 - \varepsilon_\infty)\omega\tau}{1 + \omega^2\tau^2} \tag{2}$$

where ε_0 is the static dielectric constant, ε_∞ is the dielectric constant in the limit of an infinitely high rf frequency and τ is the dielectric relaxation time. Eqs. (1) and (2) show that for $\omega\tau \ll 1$ the deposited heat increases with the square of ω, for $\omega\tau \gg 1$ the deposited power becomes independent of ω. For ions in solution the power deposited is given by [10]:

$$W_{\text{ion}} = \tfrac{1}{2}\sigma E_0^2 \tag{3}$$

where σ is the volume electric conductivity. W_{ion} is frequency independent at very low frequencies and increases with increasing frequency until $\omega\tau \approx 1$, where it reaches a plateau [10]. In a typical NMR setting, W_{ion} is the dominating contribution to power deposition, hence rf-heating is of concern mainly at higher ion concentrations.

3. Chemical shift imaging in one and two dimensions

Chemical shift imaging is routinely performed in gradient shimming, where the chemical shift of a signal is measured in a spatially resolved manner yielding a field homogeneity map [11]. The pulse sequence for one-dimensional (1D) mapping is shown in Fig. 1. It consists of a simple gradient echo sequence. After an excitation pulse the magnetization is dephased by a gradient during the phase encoding time and by the local field differences during the echo time Δ_1. A gradient of opposite sign during the acquisition period refocuses the magnetization. If we assume the gradient to be a pure z-gradient, the recorded echo contains the NMR-signal of the whole active coil length spread along the chemical shift axis. The chemical shift at each point is contained in the phase of the signal at the

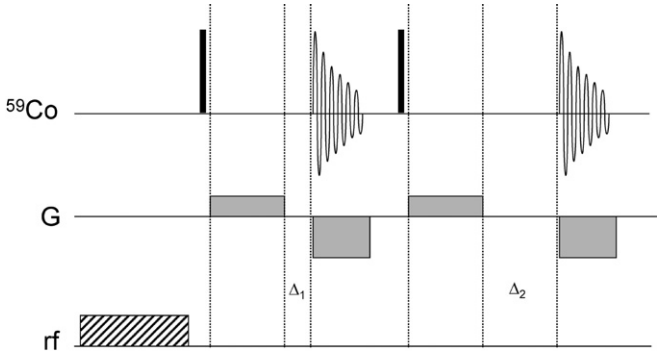

Fig. 1. Pulse sequence used for time-resolved chemical-shift mapping. Black vertical bars on the line "^{59}Co" denote radio-frequency (rf) excitation pulses at the ^{59}Co resonance frequency and the damped sine wave denotes the FID. The grey rectangles on the line "G" represent magnetic field gradients. The hatched rectangle on the line "rf" denotes a decoupling sequence. The basic pulse sequence contains a short and a long echo period, Δ_1 and Δ_2, respectively, which allows extraction of the spatial distribution of the ^{59}Co chemical shift (see text). The ^{59}Co resonance frequency has a large temperature dependence which monitors the temperature distribution resulting from rf-heating (e.g. a ^{15}N decoupling sequence or a [^{1}H,^{1}H]-TOCSY mixing sequence). Note that there was no heating applied previous to the first scan.

corresponding chemical shift. To extract this information, a second experiment with different echo time Δ_2 (but identical phase encoding/decoding) has to be recorded and the local phases must be subtracted. The resulting local phase differences correspond to the local chemical shift [11], which corresponds to the local temperature when measuring ^{59}Co.

For imaging in two dimensions different approaches are available. Their general principles are outlined in [12]. We chose to apply the projection-reconstruction method. A number of 1D-images (''projections'') are taken at different angles with the difference between the minimal and maximal angle being at least 180°. The 2D-image is calculated (''reconstructed'') from the projections. The mathematical principles for the reconstruction were first treated by Radon [13] and are described in [14].

4. Experimental

4.1. Samples

$K_3Co(CN)_6$ was obtained from Aldrich and used without further purification.

1D-temperature imaging experiments: two NMR samples were prepared, each consisting of 1 ml of an 1 M solution of $K_3Co(CN)_6$ in 90%H_2O/10%D_2O. One sample contained in addition 1.7% (w/v) agarose, which was boiled in the NMR tube in order to form a gel and thus prevent convection in the sample.

2D-xy-temperature imaging experiments: the sample consisted of a Shigemi® tube with only the central 10 mm of the tube height filled with 1 M $K_3Co(CN)_6$ in D_2O, in order not to obscure small temperature gradients in the *xy*-direction by the relatively large temperature gradients in the *z*-direction. The sample also contained 1.7% (w/v) agarose and was boiled in the NMR tube in order to form a gel. This was done to prevent convection in the sample introduced by heating.

4.2. One-dimensional (1D) temperature imaging along the z-axis

The pulse sequence for the gradient echo (Fig. 1) was supplemented with an rf-heating period (Fig. 1). The 1D-temperature imaging experiments were recorded on a BRUKER DRX600 spectrometer with a BBI probe equipped with a *z*-gradient coil. The equipment was manufactured before 1997. The echo times used were $\Delta_1 = 0.75$ ms and $\Delta_2 = 7$ ms, respectively. The acquisition time was 3.25 ms, the phase encoding gradient strength was 7.4 G/cm, the phase decoding gradient strength was −15.9 G/cm, the excitation pulse angle was 90°, the relaxation delay 450 ms, the steady-state temperature without heating was 25 °C. The transmitter frequency was set to 142.3923933 MHz. rf-heating was produced by an 80-ms clean-TOCSY sequence [15] using a rf field strength $\gamma B_1/2\pi$ of 13.9 kHz. The number of scans was set to 1. No dummy scans were used. The experiment was repeated 256 or 512 times in a pseudo-2D manner to obtain temperature distribution images at subsequent points in time.

The spatial axis was calibrated by recording 1D-images of a Shigemi® tube with a 1 mm layer of sample solution inserted into the rf coil at known positions. The calibration of the temperature axis was more elaborate: the pulse sequence shown in Fig. 1 was changed by introducing another gradient during the echo time. 1D-images were recorded at different strengths of this gradient in the range of 0.6–4.8 G/cm). The change in signal phase (relative to the center of the sample) could then be correlated to the known differences in resonance frequency introduced by the gradients, and subsequently compared to the resonance frequency shift of the ^{59}Co-signal per Kelvin of 1.23 ppm/K that we calibrated using our samples. Values of 1.45 ppm/K and 1.38 ppm/K have previously been reported [16], where it was also indicated that the chemical shift of ^{59}Co also depends on concentration and pressure. As a consequence of the imaging method used, the phase difference between the two experiments at the central point is always zero. Thus the apparent temperature difference at this point in space is 0 for temperature images recorded at different times during the heating sequence and the temperature curve obtained has to be shifted along the temperature axis. To determine the amount by which the profile needed to be shifted along the temperature axis, a series of standard 1D ^{59}Co spectra was recorded with identical heating power to that used for the imaging between the 1D-spectra, The average sample temperature could be calculated from the 1D-spectra. In the last step, each of the temperature profiles was shifted along the temperature axis in order to reach an average temperature corresponding to the average temperature at the same point in time obtained from the series of 1D-spectra.

Time-resolved 1D-temperature profiles along the *z*-axis were measured under different conditions: with rf applied to the ^{1}H or the X-coil of the probe double-tuned to the frequency of ^{59}Co and of ^{15}N, with and without temperature regulation, with 400 L/h and without airflow. These measurements were performed on both the sample with and the one without agarose gel.

4.3. Two-dimensional (2D) temperature imaging in the xy-plane

2D-*xy*-images were recorded by the Projection–Reconstruction method, in which a set of 1D-images (''projections'') with different orientations of the projection axis is recorded and the 2D-image is calculated (''reconstructed'') from this set of 1D-images, referred to as ''shadows''. The experiment for 1D-temperature imaging described above (Fig. 1) was repeated up to 32 times with different orientations of the projection axes. Between the measurements of two projections a time period of 20 min was provided for the sample to cool completely and reach the equilibrium temperature. (1D-^{59}Co spectra measured at 30 s intervals during the waiting demonstrated that equilibrium was

usually reached after 6 min already.) The number of projections chosen was a compromise between measuring time and necessary resolution. In order to maximize sensitivity, which is especially important at the horizontal edges of the sample, several scans were accumulated with an optimized ratio of the recycling delay (≈90 ms) and the pulse angle (63°) [17]. Under the experimental conditions used here, the longitudinal and transverse relaxation time of ^{59}Co nuclear spins in $K_3Co(CN)_6$ was $T_1 \approx 100$ ms and $T_2 \approx 32$ ms, respectively. A CYCLOPS phase cycle was used to eliminate quadrature artifacts (digital-quadrature-detection was not available for the large spectral widths employed). One 1D-temperature image was recorded every second, whereof 80 ms were used for WALTZ-16 decoupling (heating) on ^{15}N with a field strength $\gamma B_1/2\pi$ of 2.4 kHz. When 1 s per image would not provide adequate time resolution, the measurement time per temperature image can be reduced to <300 ms. The data structure obtained when running a row of 1D-*xy*-heating imaging measurements using the pulse sequence of Fig. 1 with changing orientation of the projection axis in the *xy*-plane is shown in Fig. 2 and explained in the figure caption.

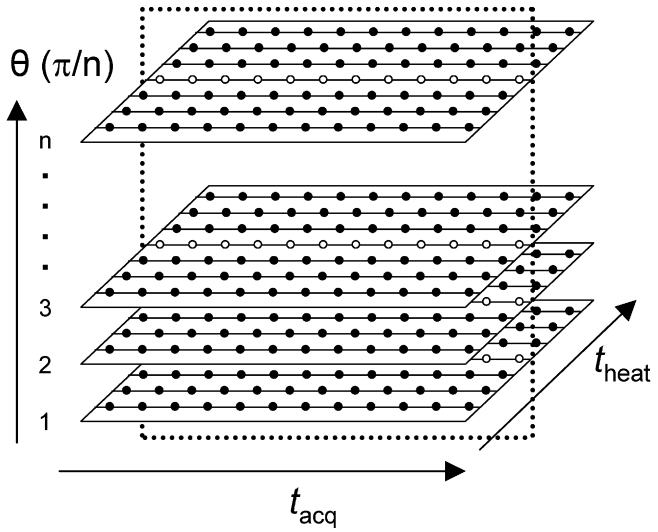

Fig. 2. Data structure of the real-time two-dimensional (2D) imaging experiment representing the temperature distribution across the sample. The experiment was recorded in a pseudo three-dimensional (3D) manner. One-dimensional (1D) chemical-shift maps, recorded with the pulse sequence shown in Fig. 1, constitute the acquisition dimension, t_{acq}. The signal represents a spatially resolved chemical shift of ^{59}Co, corresponding to the average chemical shift in the slice perpendicular to the axis defined by the gradients in Fig. 1. The spatial distribution of ^{59}Co chemical shifts is equivalent to the temperature distribution. The measurements were carried out in a rapid sequence, applying heating through the application of rf irradiation (Fig. 1). The FIDs collected with this procedure constitute the "heating dimension", t_{heat}. After recording one (t_{acq}, t_{heat})-plane, a 20 min waiting period allowed the sample to cool to the initial steady-state temperature. Then an analogous heating experiment was recorded with the angle θ of the *xy*-gradient rotated about the *z*-axis. The experiment was repeated until a total rotation of exactly 180° about the *z*-axis was obtained and the third dimension, θ was thus completed. The data containing the information on the 2D-chemical shift distribution at a given time, t_{heat}, after the heating was started is contained in a plane spanned by the dimensions t_{acq} and θ at t_{heat}. Such a plane is indicated in the figure by the dotted rectangle and the open circles for individual data points contained in this plane. After reconstruction the 2D-chemical shift image was converted to a 2D-temperature distribution map as described in the text.

The steady-state *xy*-temperature distribution in the sample was measured after an initial period of 20 min during which steady-state was reached. Then, 1D-temperature images along different projection axes were taken while maintaining rf-heating. This situation corresponds to lengthy experiments involving rf-heating.

Sample cooling was imaged by first heating the sample to a steady-state temperature distribution, then switching off the heating and recording a series of time-resolved 1D-*xy* temperature profiles at different projection angles. Each of the separately recorded 1D-*xy* temperature distribution images was evaluated, the data sets were combined and a time slice was extracted as illustrated in Fig. 2.

The *xy*-imaging experiments were recorded on a BRUKER DRX500 spectrometer with a specially adapted triple resonance probe tuned to ^{1}H, ^{15}N and ^{59}Co) equipped with a *xyz*-gradient coil, manufactured before 1997. However, the experiments can be recorded using any broadband-tuneable probe equipped with triple-axis gradients. During all experiments active temperature regulation was applied using an airflow of 400 L/h.

A published Mathematica® algorithm for the reconstruction of 2D-intensity images from a set of 1D-intensity images [18] was adapted for our needs by (i) allowing for different resolutions in the space and angle dimensions, (ii) incorporating routines to import and handle experimental data, (iii) preparing the measured projections for image reconstruction, (iv) providing routines for the graphical representation of the results.

5. Results and discussion

5.1. 1D-heating images along the z-axis

Fig. 3 shows the temperature profile of the sample along the *z*-axis. The temperature at each point along the *z*-axis represents the average temperature in the transverse plane. The temperature is plotted against experimental time to monitor the chemical shift of ^{59}Co in $K_3Co(CN)_6$ during the heating experiment. Fig. 3a shows the temperature profile without temperature regulation. A parabolic temperature distribution developed, resulting from spatially homogeneous heating with heat dissipation at the boundaries of the active coil region. At the warmest point, the temperature increased by 6.25 K during the experiment.

Fig. 3b shows the same experiment with temperature regulated air flow from the negative *z*-direction. The temperature profile has changed from that observed without temperature regulation. The region with the highest temperature was now shifted upwards and was located approximately 7 mm above the center of the coil while the parabolic temperature distribution became asymmetric. The overall temperature increase was reduced to 1.53 K at the warmest point.

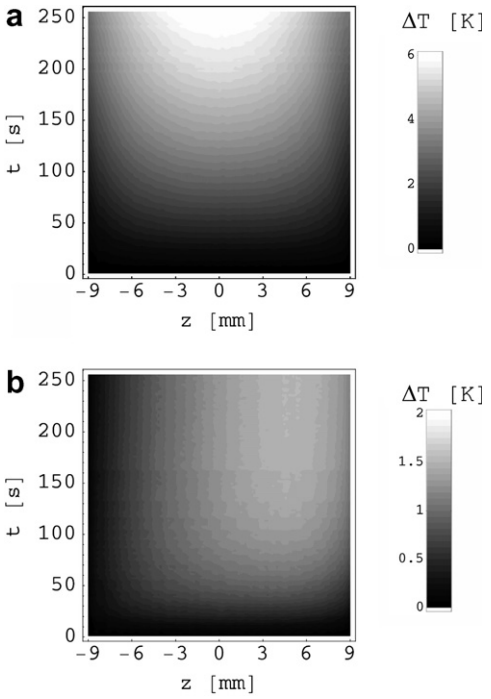

Fig. 3. Temperature profiles along the z-axis of cylindrical samples plotted against the heating time, t. The data were recorded with the pulse sequence shown in Fig. 1, using a total time of 1.179 s for each profile, including 200 ms of rf-heating. The heating was accomplished by a WALTZ-16 sequence with a field strength $\gamma B_1/2\pi$ of 1.25 kHz at the resonance frequency of ^{59}Co. The experiment was performed on a BRUKER DRX600 with a broadband inverse detection (BBI) probe equipped with a with magnetic field gradient coil along the z-axis. The sample contained 1 M $K_3Co(CN)_6$ in a 1.7% (w/v) agarose gel. The space coordinate z ranges from -9 to +9 mm, corresponding to the active length of the rf coil in the probe; negative values denote a position below the center of the coil. Time-dependent local temperatures are indicated by gray tones according to the temperature scale shown on the right. (a) Shows temperature profiles in the absence of a cooling air flow (i.e. no temperature regulation). A parabolic temperature distribution developed corresponding to spatially homogeneous heating and heat dissipation at the boundaries of the active coil region. At the warmest point, the temperature increased 6.25 K during the experiment. (b) Shows results from the same experiment with a temperature regulated air flow from the negative z-direction. In contrast with (a) the temperature profile showed that the region with the highest temperature was approximately 7 mm above the center of the coil and the parabolic temperature distribution had become asymmetric. The overall temperature increase at the warmest point was reduced to 1.53 K.

The shift in the location of the temperature maxima clearly indicates that they are not the result of inhomogeneity of the applied rf-fields, but resulted from temperature regulation and equilibration with the surrounding at the edge of the actively heated regions. This view is supported by the first few profiles in Fig. 3a which were homogenous along the z-axis for short times t, when heat conduction was still negligible. For the measurements shown in Fig. 3 convection in the sample was limited by the use of a 1.7% (w/v) agarose gel. A measurement without gel showed nearly the same results, indicating that the combination of solution viscosity, sample tube dimensions and temperature differences during the experiments was such, that no significant convection took place (see [1] on convection in NMR sample tubes). Standard conditions used in NMR measurements with biological macromolecules in aqueous solution use temperature regulation and allow free convection, conditions in which we observe temperature gradients up to 1.5 K in the sample over the active volume of the ^{59}Co coil (Fig. 3b).

5.2. Time-resolved 2D-heating images in the xy-plane

Fig. 4 shows a series of time-resolved 2D- temperature profiles of a 1 M aqueous solution of $K_3Co(CN)_6$ using a Shigemi® (Shigemi Inc.) tube with a sample height of 10 mm. The solution contained 1.7% (w/v) agarose to prevent thermal convection. A series of measurements with a time resolution of 1 s was taken during a heating sequence with active temperature regulation. In general, there were only small temperature differences across the 2D-temperature profiles. With the experimental parameters used (see Fig. 4), the temperature differences were at most 0.2 K. During the first 20 s of the rf-heating process, two distinct regions appear to experience stronger rf-heating than the average across the sample. These two regions are located at opposite edges of the sample, approximately on the 45° line in the coordinate system defined by the gradient coils. This effect was detected only at the beginning of the heating sequence (Fig. 4); later it was obscured by heat conduction (Fig. 5). Note that the data points at the edges of the images show lower values – an artifact originating from the digitization of the spatial coordinates.

5.3. 2D steady-state temperature distribution in the xy-plane

Fig. 5 shows the temperature distribution in the xy-plane after reaching the steady-state in a NMR experiment with a heating sequence. The temperature profiles in the xy-plane show at each point the average temperature along the z-axis of the sample. There was a significant deviation from the expected [19] parabolic temperature profile. In Fig. 5, a warmer area is detected at one edge of the sample, located at the bottom left of the image. This result was similar to the steady-state temperature distribution shown by Loening and Keeler [6]. A single temperature profile does not allow one to distinguish whether the effect arose from inhomogeneous heating or from inhomogeneous cooling. (Even small deviations of the sample position from the center of the cylindrical geometry might cause different efficiencies of sample cooling on different sides of the sample). Further insight was gained by repeating the steady-state heating experiment several times. First, an estimation of the accuracy of the method was obtained by measuring the steady-state temperature profile several times without moving the sample. These experiments yielded identical results (data not shown). In a second series of measurements the sample was rotated to a different position between the measurements of the different

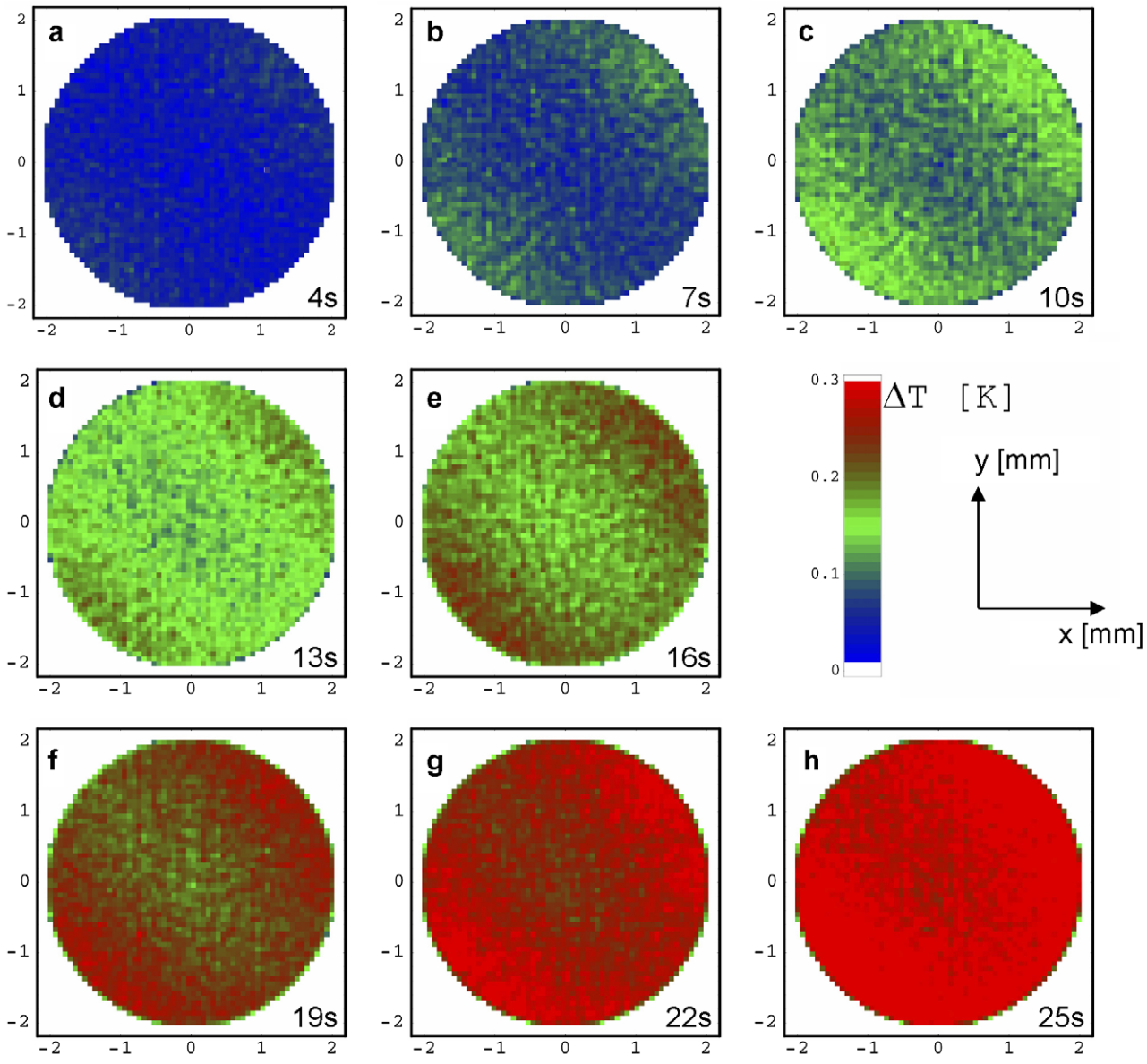

Fig. 4. Selected 2D-images of the temperature distribution perpendicular to the NMR tube axis from a real-time heating experiment measured with the pulse sequence shown in Fig. 1. The sample contained 1 M $K_3Co(CN)_6$ in 95% H_2O/5% D_2O. A Shigemi® (Shigemi Inc.) tube was used. The sample height was 10 mm and the sample was centered in the active coil region. Thirty-two projections were recorded with equidistant angles of the projection axis (angles: $0° + n*5.625°$, $n = 0 \ldots 31$) relative to the x axis of the magnetic field gradient coil. The individual projections contain 512 data points, of which only the central 62 contained data. These 62 data points cover the inner diameter of 4.06 mm and are subsequently converted to a spatial axis ranging from −2.03 to +2.03 mm. Thus the image has a spatial resolution of 65μm/pt. The rf-heating was accomplished by an 80 ms WALTZ-16 decoupling with a field strength of $\gamma B_1/2\pi = 2.4$ kHz which was applied at the ^{15}N frequency on a BRUKER DRX500. The BRUKER temperature regulation unit BVT-3000 including a BCU05 cooling device was used with an airflow of 400 L/h and temperature regulation for a target temperature of 295 K. The panels show the temperature distribution in the sample after the following time periods: (a) 4 s, (b) 7 s, (c) 10 s, (d) 13 s, (e) 16 s, (f) 19 s, (g) 22 s and (h) 25 s after switching on heating, as indicated in the lower right corner of the individual panels. One full 2D-temperature image was recorded every second, thus the data points shown here represent only every third recorded temperature image.

temperature images. The results are shown in Fig. 5. The overall picture remained unchanged: a warmer area was observed in the third quadrant near to the negative y-axis together with a temperature gradient across the sample. However, the experiments did not yield identical temperature distribution images. Both the exact position of the warm area and especially the colder area, as well as the temperature gradient across the sample, varied. These measurements suggest that the exact sample position caused the differences observed. There is an area at the edge of the tube with slightly stronger cooling, but this area changes when the sample is moved. On the other hand, the warmer area does not move by more than 15°. This observation could be attributed to inhomogeneous rf-heating, which seems unlikely when the results shown in Fig. 4 are taken into consideration, or to inhomogeneous sample cooling

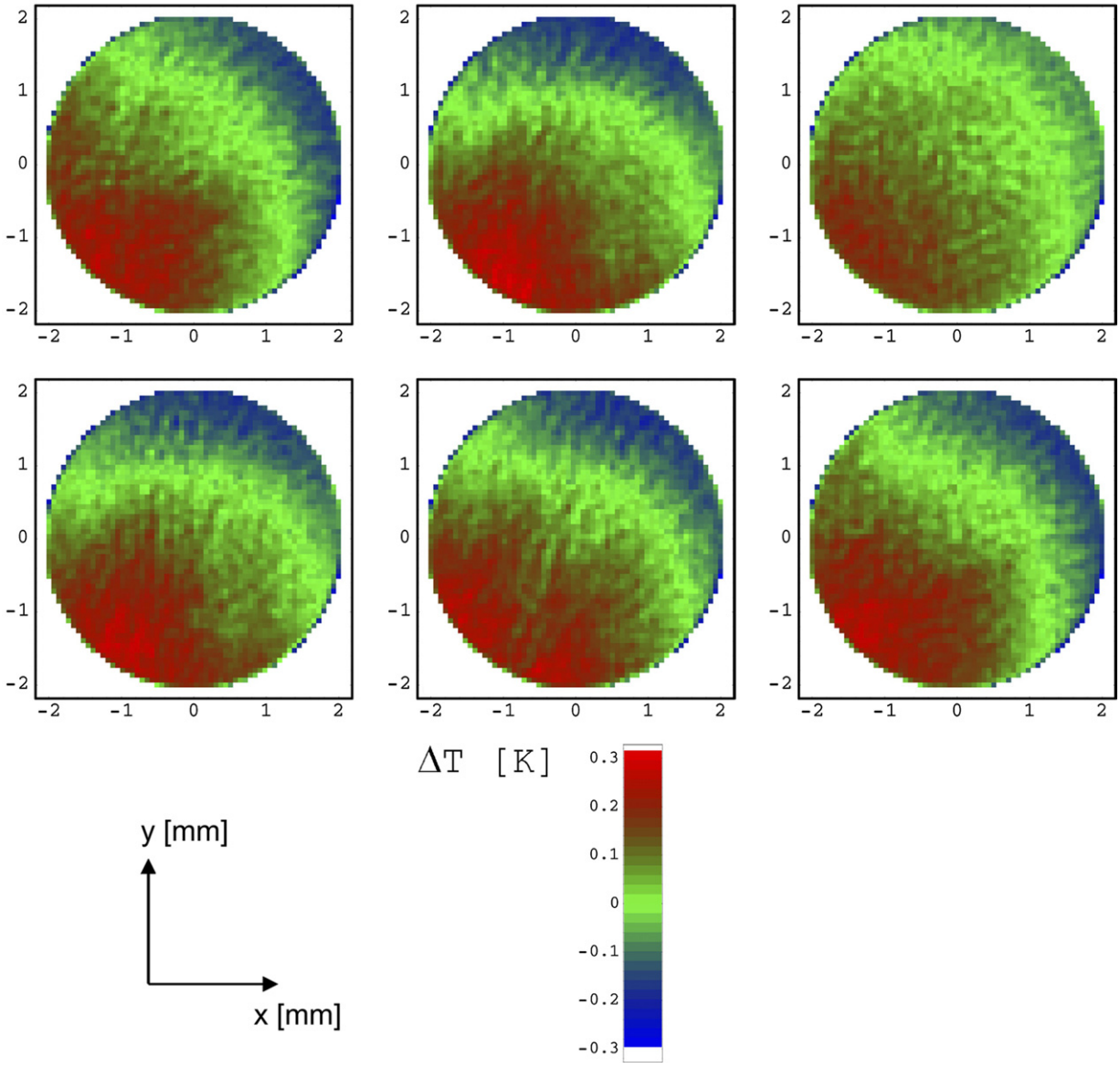

Fig. 5. 2D-images of the temperature distribution perpendicular to the NMR tube axis after reaching the steady-state in the experimental setup described in Fig. 4. This situation corresponds to a typical NMR experiment with decoupling and temperature regulation. The temperature gradient across the sample is not caused primarily by inhomogeneous rf-heating, but by inhomogeneous cooling (see text). Six experiments were performed with identical heating/cooling conditions. Between the measurements, the sample was spun for an arbitrary time ranging from 10 to 30 s. The six panels show the steady-state temperature distribution for the six experiments. The scale is adjusted such that $\Delta T = 0$ denotes the average temperature of all six samples.

caused by an uneven distribution of the cooling gas around the sample tube. The latter problem would depend on the exact geometry of the probe.

5.4. Time resolved temperature profiles in the xy-plane during cooling down

Fig. 6 shows the changing temperature distribution when the sample is cooled, starting from a steady-state-temperature distribution (Fig. 6a) as described in the caption of Fig. 5. For this series of measurements the same sample was used as for Fig. 5 and the temperature regulation was active. After switching off the heating, the temperature profile approached a uniform distribution of temperatures throughout the sample. No obvious dominant spatial inhomogeneity of the cooling process could be observed from the data.

6. Conclusion

The procedure presented in this work permits measurement of temperature profiles, which are resolved in one or two spatial dimensions, in real-time by NMR. The method can be used to follow the temperature changes during heating or cooling of a solution. For high-resolution NMR spectrometers, we can conclude from our data that both the rf-heating and the sample cooling produce an inhomogeneous temperature distribution across the sample,

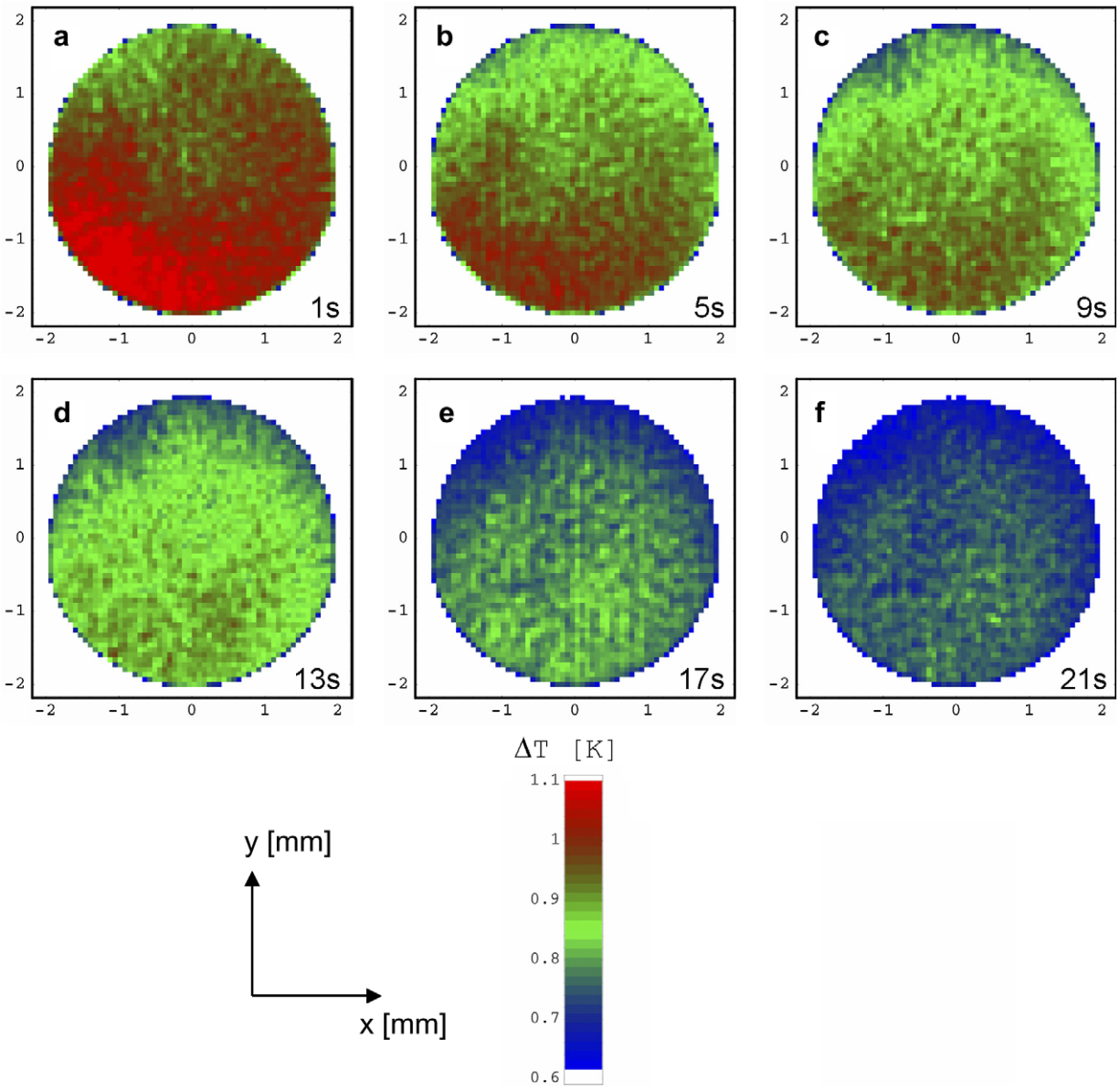

Fig. 6. 2D-images of the temperature distribution perpendicular to the NMR tube axis obtained after switching off rf-heating after a steady-state temperature distribution had been obtained with rf-heating, as shown in Fig. 5. The rf-heating was switched off while temperature regulation with a target temperature of 295 K using an airflow of 400 L/h was maintained. For better visibility, the temperature bar is scaled such, that $T = 0$ refers to the equilibrium temperature in the sample reached after 128 s. The images were taken at the following times: (a) 1 s, (b) 5 s, (c) 9 s, (d) 13 s, (e) 17 s, and (f) 21s after switching off rf-heating, as indicated in the lower right corner of the individual panels.

irrespective of the use of the spectrometer's temperature regulation. Inhomogeneous rf-heating originates from a non-uniform electric field inside the rf coil. Inhomogeneous sample cooling arises from an unequal distribution of cooling air on the surface of the sample. A slightly asymmetric positioning of the (non-spinning) spinner or inhomogeneous cooling air supply will also contribute to inhomogeneous cooling. In our experiments we used a sample with a high ionic strength, but applied moderate rf-heating sequences. Under these conditions the temperature differences across the *xy*-plane of the NMR sample did not exceed 0.6 K (Fig. 5) in steady-state conditions, but in the *z*-direction of the sample temperature differences reached 1.5 K.

The method for real-time measurements of temperature profiles is applicable on every broadband-tuneable probe equipped with the necessary magnetic field gradients and is not limited to analytical NMR. It can easily be used e.g. for MRI using an appropriate phantom. The temperature profiles provide an estimation of peak temperatures and their localization in the sample, which is of prime importance when working with temperature-sensitive samples, especially also for *in vivo* NMR. Furthermore, the method makes possible a quantification of temperature

gradients within an NMR sample during an NMR experiment. The temperature profiles could also become a valuable tool in the development of new coil geometries for NMR probes. The profiles provide an experimental verification of numerical simulations of the electric fields occurring in coils.

Acknowledgments

We thank Prof. K. Wüthrich for his interest and support of this work. We thank Oskar Schett, Daniel Marek, Michael Warden and Roberto Seydoux for valuable discussions. BRUKER Biospin AG, Fällanden (Switzerland) is acknowledged for financial support and providing a triple-gradient ^{59}Co-tuned probehead. Financial support from the Swiss National Science Foundation (SNF) and the KTI, Project No. 3392.1 is gratefully acknowledged. We thank Marilyn Wiebe for editing the manuscript.

References

[1] N. Hedin, I. Furó, Temperature imaging by ^{1}H NMR and suppression of convection in NMR probes, J. Magn. Reson. 131 (1998) 126–130.
[2] N.M. Loening, J. Keeler, Measurement of convection and temperature profiles in liquid samples, J. Magn. Reson. 139 (1999) 334–341.
[3] A. Jerschow, Thermal convection currents in NMR: flow profiles and implications for coherence pathway selection, J. Magn. Reson. 145 (2000) 125–131.
[4] A. Jerschow, N. Müller, Suppression of convection artifacts in stiumlated-echo diffusion experiments: double-stimulated-echo experiments, J. Magn. Reson. 125 (1997) 372–375.
[5] A. Jerschow, N. Müller, Convection compensation in gradient enhanced nuclear magnetic resonance spectroscopy, J. Magn. Reson. 132 (1998) 13–18.
[6] N.M. Loening, J. Keeler, Temperature accuracy and temperature gradients in solution-state NMR spectrometers, J. Magn. Reson. 159 (2002) 55–61.
[7] H. Quast, M. Heubes, A. Dunger, H.-H. Limbach, A high-precision Carbon-13 shift thermometer for the temperature range 100–300 K, J. Magn. Reson. 134 (1998) 236–244.
[8] J. Saunavaara, J. Jokisaari, Determination of sample temperature and temperature stability with ^{129}Xe NMR, J. Magn. Reson. 180 (2006) 58–62.
[9] G.C. Levy, J.T. Bailey, D.A. Wright, A sensitive NMR thermometer for multinuclei FT NMR, J. Magn. Reson. 37 (1980) 353–356.
[10] J.J. Led, S.B. Petersen, Heating effects in Carbon-13 NMR spectroscopy on aqueous solutions caused by protein noise decoupling at high frequencies, J. Magn. Reson. 32 (1978) 1–17.
[11] R. Kimmich, NMR. Tomography, Diffusometry, Relaxometry, Springer, 1997.
[12] R.R. Ernst, G. Bodenhausen, A. Wokaun, Principles of Nuclear Magnetic Resonance in One and Two Dimensions, Clarendon Press, Oxford, 1989.
[13] J. Radon, Über die Bestimmung von Funktionen durch ihre Integralwerte längs gewisser Mannigfaltigkeiten, Berichte Sächsische Akademie der Wissenschaften. Leipzig, Math. Phys. Kl. 69 (1917) 262–267.
[14] A.C. Kak, M. Slaney, Algorithms for reconstruction with nondiffracting sources, in: Principles of Computerized Tomographic Imaging, IEEE Press, New York, 1988, pp. 49–112.
[15] C. Griesinger, G. Otting, K. Wüthrich, R.R. Ernst, Clean TOCSY for ^{1}H spin system identification in macromolecules, J. Am. Chem. Soc. 110 (1988) 7870–7872.
[16] W.J. Goux, L.A. Verkruyse, S.J. Salter, The impact of Rayleigh–Benard convection on NMR pulsed-field-gradient diffusion measurements, J. Magn. Reson. 88 (1990) 609–614.
[17] R.R. Ernst, Sensitivity enhancement in magnetic resonance, Adv. Magn. Reson. 2 (1966) 1–135.
[18] H. Murrell, Computer-aided tomography, Math. J. 6 (1996) 60–65.
[19] W.J. Beek, K.M.K. Mutzall, Transport Phenomena, John Wiley & Sons Ltd., London, 1975.